BMC Musculoskeletal Disorders

RESEARCH

Open Access

Anterior percutaneous full-endoscopic transcorporeal decompression for cervical disc herniation: a finite element analysis and long-term follow-up study

Qian Du[1,3†], Zheng-Ji Wang[1,3†], Hai-Dong Zheng[1,3], Shu-Fa Wang[1,3], Guang-Ru Cao[1,3], Zhi-Jun Xin[2,3], Min-Bo Zhang[1,3], Wei-Jun Kong[1,3*] and Wen-Bo Liao[1,3*]

Abstract

Objective The purpose of this study was to investigate the long-term consequences on the cervical spine after Anterior transcorporeal percutaneous endoscopy cervical discectomy (ATc-PECD) from the biomechanical standpoint.

Methods A three-dimensional model of the normal cervical spine C2-T1 was established using finite element method. Subsequently, a disc degeneration model and degeneration with surgery model were constructed on the basis of the normal model. The same loading conditions were applied to simulate flexion, extension, lateral bending and axial rotation of the cervical spine. We calculated the cervical range of motion (ROM), intradiscal pressure, and intravertebral body pressure under different motions for observing changes in cervical spine biomechanics after surgery. At the same time, we combined the results of a long-term follow-up of the ATc-PECD, and used imaging methods to measure vertebral and disc height and cervical mobility, the Japanese Orthopaedic Association (JOA) score and visual analog scale (VAS) score were used to assess pain relief and neurological functional recovery.

Results The long-term follow-up results revealed that preoperative JOA score, neck VAS score, hand VAS score, IDH, VBH, and ROM for patients were 9.49 ± 2.16, 6.34 ± 1.68, 5.14 ± 1.48, 5.95 ± 0.22 mm, 15.41 ± 1.68 mm, and 52.46 ± 9.36° respectively. It changed to 15.71 ± 1.13 ($P < 0.05$), 1.02 ± 0.82 ($P < 0.05$), 0.77 ± 0.76 ($P < 0.05$), 4.73 ± 0.26 mm ($P < 0.05$), 13.67 ± 1.48 mm ($P < 0.05$), and 59.26 ± 6.72° ($P < 0.05$), respectively, at 6 years postoperatively. Finite element analysis showed that after establishing the cervical spondylosis model, the overall motion range for flexion, extension, lateral bending, and rotation decreased by 3.298°, 0.753°, 3.852°, and 1.131° respectively. Conversely, after establishing the bone tunnel model, the motion range for these actions increased by 0.843°, 0.65°, 0.278°, and 0.488° respectively, consistent with the follow-up results. Moreover, analysis of segmental motion changes revealed that the increased

†Qian Du and Zheng-Ji Wang contributed equally to this work and share first authorship.

*Correspondence:
Wei-Jun Kong
kong0526@sina.com
Wen-Bo Liao
wenbo900@sina.com

Full list of author information is available at the end of the article

© The Author(s) 2024. **Open Access** This article is licensed under a Creative Commons Attribution-NonCommercial-NoDerivatives 4.0 International License, which permits any non-commercial use, sharing, distribution and reproduction in any medium or format, as long as you give appropriate credit to the original author(s) and the source, provide a link to the Creative Commons licence, and indicate if you modified the licensed material. You do not have permission under this licence to share adapted material derived from this article or parts of it. The images or other third party material in this article are included in the article's Creative Commons licence, unless indicated otherwise in a credit line to the material. If material is not included in the article's Creative Commons licence and your intended use is not permitted by statutory regulation or exceeds the permitted use, you will need to obtain permission directly from the copyright holder. To view a copy of this licence, visit http://creativecommons.org/licenses/by-nc-nd/4.0/.

cervical spine mobility was primarily contributed by the surgical model segments. Additionally, the finite element model demonstrated that bone tunneling could lead to increased stress within the vertebral bodies and intervertebral discs of the surgical segments.

Conclusions Long-term follow-up studies have shown that ATc-PECD has good clinical efficacy and that ATc-PECD can be used as a complementary method for CDH treatment. The FEM demonstrated that ATc-PECD can lead to increased internal stresses in the vertebral body and intervertebral discs of the operated segments, which is directly related to cervical spine degeneration after ATc-PECD.

Keywords Anterior transcorporeal percutaneous endoscopic cervical discectomy, ATc-PECD, Finite element analysis, Biomechanics, Long term follow up

Introduction

With the increasing popularity of minimally invasive techniques, percutaneous endoscopic cervical discectomy (PECD) has been a widely used treatment for cervical disc herniation (CDH) [1]. PECD can be performed through two different approaches: anterior or posterior. Anterior transdiscal percutaneous endoscopic cervical decompression (ATd-PECD) is the first introduced cervical PECD technique, which utilizes a percutaneous endoscopic approach through the intervertebral disc. ATd-PECD avoids the loss of motion segments caused by traditional open surgery's fusion of vertebral bodies while also reducing the risk of various complications associated with traditional open surgery [2]. However, the iatrogenic injury to the intervertebral disc caused by ATd-PECD can lead to a significant decrease in intervertebral disc height (IDH) [3]. In addition, this approach is not suitable for patients with low IDH or anterior vertebral space osteophyte [3, 4]. In order to avoid damage to the normal intervertebral disc structures anteriorly, Ruetten et al. proposed in 2007 to utilize a full-endoscopic approach from the posterior cervical region through the interlaminar space to decompress [5]. However, posterior percutaneous endoscopic cervical decompression (P-PECD) is more suitable for decompressing the lateral spinal cord or nerve roots compressions. It is not applicable for compressions located anteriorly to the spinal cord. George et al. first proposed the anterior transcorporeal technique in 1993 [6]. Subsequently, various surgeons have made different improvements based on this technique. However, all these surgical modifications were performed under either microscopic or open surgical conditions, all of which were to some extent limited by issues such as surgical field obscuration or complications associated with open surgery [7–9]. In order to overcome the limitations associated with the aforementioned surgical approaches, Deng et al. and Liao et al. pioneered the combination of full-endoscopic technology with transcorporeal techniques, introducing the anterior transcorporeal percutaneous endoscopic cervical decompression (ATc-PECD) procedure [10, 11]. ATc-PECD creates a bony channel in the vertebral body that reduces interference to the intervertebral space by bypassing the normal intervertebral disc in front of the lesion area. Moreover, it also allows for a wider range of depressurization by adjusting the exit direction and larger channel diameters. In our preliminary study, we have confirmed the excellent clinical efficacy of ATc-PECD in the treatment of CDH [11–14].

Mechanical loading is pivotal in the progression of cervical disc degeneration [15]. Moreover, it can disturb the metabolic remodeling of bone tissue by promoting osteoclast differentiation and impeding osteoblast differentiation [16]. In ATc-PECD procedure, the bony channel in the vertebral body can alter the inherent pathways of stress transmission in the cervical spine, ultimately leading to atypical concentration of stress in the cervical [17]. Hence, the establishment of bone channel may potentially promote the degenerative changes of vertebral body and intervertebral disc [11, 18].

The finite element model (FEM) is a valuable tool in biomechanical research, which enables the observation the postoperative tissue biomechanical changes through computer modeling and simulation [19]. In the previous studies that utilized FEM to investigate the biomechanics of cervical spine following the establishment of bone channel have primarily focused on immediate outcome, such as the risk of vertebral body fractures and the changes of cervical spine mobility after surgery [17, 20]. Additionally, the initial construction of the FEM in these studies did not take into account the biomechanical changes in the cervical spine caused by disc degeneration. So, further research is needed to comprehensively understand the long-term implications of transcorporeal bone channel on the biomechanics of the cervical spine.

The existing clinical studies on ATc-PECD has primarily consisted of short-term follow-up observations [11, 13, 21], the long-term clinical outcomes are still unreported. To advance the understanding in this field, our research team conducted a long-term follow-up study on patients who underwent ATc-PECD for single-segment CDH. In addition, we integrated a finite element analysis (FEA) study into our study to elucidate the effects of

ATc-PECD on the cervical spine from a biomechanical perspective.

Materials and methods

Establishment of complete FEM

In this study, we adopted the modeling approach described by Wang et al. [22]. to construct a 3D FEM of the C2-T1 cervical region. The transverse cryosections from the Chinese Visible Human 2 dataset were utilized to delineate the boundaries of soft tissues and bones. These cryosections were obtained from a 22-year-old female cadaveric donor with a weight of 52 kg and a height of 162 cm. Transverse cryosection images were selected from layers 1584 through 1792 of the dataset, with a layer spacing of 0.25 mm. The original color images of the cervical spine structures were manually segmented by a spine surgeon and an anatomist using Adobe Photoshop (version CC 2018, Adobe Systems, San Jose, Calif). The image segmentation quality and model surface smoothing were verified using Amira software (version 5.3.3, Visage Imaging, Carlsbad, CA). Refinement and mesh generation of the model were performed based on the obtained surface files using Hyper Mesh software (version 12.0, Altair, Michigan).

The intact FEM (Fig. 1) includes the vertebral body, intervertebral disc, ligaments, and articular cartilage. In constructing the vertebral body model, we differentiated between cortical bone and cancellous bone due to their distinct physical properties. The thickness of cortical bone was determined according to the study by Panjabi et al [23, 24].

Vertebral cartilage consists of zygapophysial joint cartilage and endplate cartilage. The thickness of the zygapophysial joint cartilage was determined based on the study conducted by Womack et al [25]. In the model, the surface contact algorithm was employed to simulate the zygapophysial joint, with a friction coefficient assumed to be 0.1 [26]. The endplate cartilage serves as a connecting structure between the vertebral body and the fibrous annulus of the intervertebral disc. We set the central height of the endplate cartilage at 0.6 mm and gradually increased it to 1.2 mm outward, following previous studies [27].

The intervertebral disc is composed of the nucleus pulposus and the outer annulus fibrosus, with a volume ratio of 4:6 between them [28, 29]. The nucleus pulposus was modeled as a hyperelastic, incompressible material, and its mobility was simulated using a two-parameter Mooney-Rivlin formula. The annulus fibrosus consists of concentric fiber laminae and a ground substance. The ground substance was represented by a two-node, tension-only, nonlinear spring element. The fibers were arranged in eight concentric rings, which accounted for 20% of the total volume of the fiber rings. (Figs. 1)

Following the creation of a mesh model for the vertebral body and intervertebral disc, the ligaments were constructed based on the model, ensuring connection to the vertebral body in accordance with anatomical features. Two-node, tension-only, nonlinear spring elements were employed to model all the ligaments. The modeling parameters for all the aforementioned structures are presented in (Table 1).

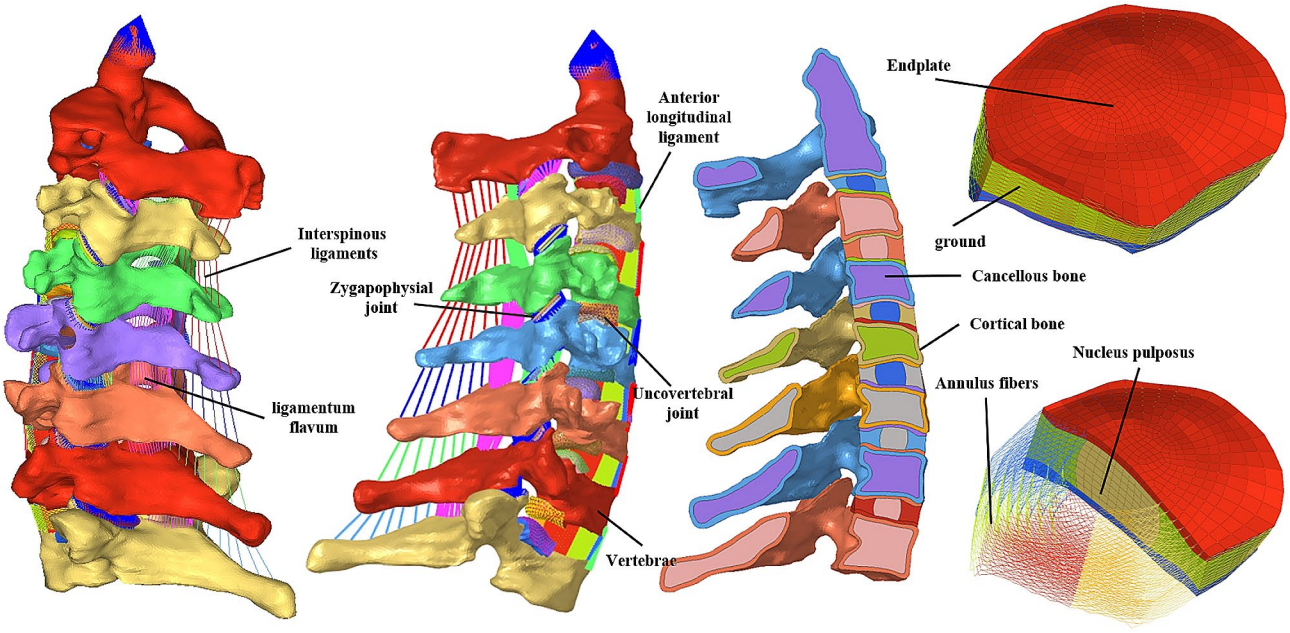

Fig. 1 Finite element model of intact C2–T1 and components

Table 1 Material properties of model components

Name	Element Type	Material Model	Material property	Reference
Cancellous bone	C3D4	Isoelastic	E = 100 MPa μ = 0.3	[30]
Cortical bone	C3D4	Isoelastic	E = 8000 MPa μ = 0.3	[30]
Cartilaginous end-plate	C3D8	Isoelastic	E = 23.8 MPa μ = 0.3	[31]
Cartilage of zygapophysial joint	C3D8	Isoelastic	E = 23.8 MPa μ = 0.3	[31]
Nucleus	C3D8H	Hyperelastic	C10 = 0.12, C01 = 0.09	[31]
Annulus ground substance	C3D8H	Hyperelastic	C10 = 0.133, C01 = 0.0333, D = 0.6	[27, 32]
Annulus fiber	Spring A	Nonlinear spring	Stress–strain curve	[31, 33, 34]
ligaments	Spring A	Nonlinear spring	Force–defection curve	[35, 36]

Material properties assumed for initial model and ATc-PECD model. E: Young modulus; μ: Poission's ratio

Establishment of the degenerative and bony channel FEM

CDH is commonly correlated with different levels of disc degeneration. Under the combined influence of various physiological and physical factors, intervertebral disc degeneration involves a process where nucleus pulposus cells gradually undergo apoptosis, matrix synthesis decreases, degradation increases, and the water content of the nucleus pulposus diminishes. Eventually, this leads to a reduction in intervertebral disc height [37, 38]. To enhance the accuracy of our FEA, we replicated intervertebral disc degeneration by reducing the disc height of the C4/5 segment by 25% in the complete finite element model. The reduction in disc height was proportionally applied. (Figure 2a and b) Surgical injury to the target segment's intervertebral disc was not simulated. Subsequently, we developed a transcorporeal bone approach model based on this modified FEM model. Considering the prevalence of CDH, the fifth cervical vertebra was chosen as the surgical model. Based on our preliminary study, the diameter of the bone channel was set at 6.9 mm [13, 39, 40]. The entrance of the bone channel is located near the anterior inferior edge of the C5 vertebral body, starting from the central anterior surface of the distal end of the C5 vertebral body and inclining upward along the interior of the vertebral body to reach the upper posterior edge of the vertebral body. (Figs. 2c) At the exit point, partial endplates are excised. The anterior longitudinal ligament and posterior longitudinal ligament are partially damaged but not completely disrupted.

Boundary and loading conditions

The loading conditions remained consistent throughout the intact model, the disc degeneration model, and the degeneration plus surgery model. The inferior surface of the T1 vertebra was immobilized, while an experimental load was exerted on the upper portion of the C2 vertebra. A vertical force of approximately 50 N was employed to simulate the weight of the human head [17]. Furthermore, a torque of 2 Nm was applied in the directions of flexion, extension, rotation, and lateral bending to replicate cervical motion [22].

Patients selection

This study received approval from the local ethics committee, and all patients provided informed consent. The inclusion criteria were as follows: (1) patients with single segment central or paracentral CDH; (2) patients who did not experience improvement or had worsening symptoms after 4 weeks of standard conservative treatment; (3) presence of neurological symptoms consistent with preoperative imaging; (4) mild cervical spondylosis of the spinal cord (Nurick grade III or below); (5) no cervical instability; (6) adherence to a follow-up period of more than 6 years. The exclusion criteria were as follows: (1) patients with multi-segment CDH; (2) patients with lateral posterior CDH; (3) patients with cervical

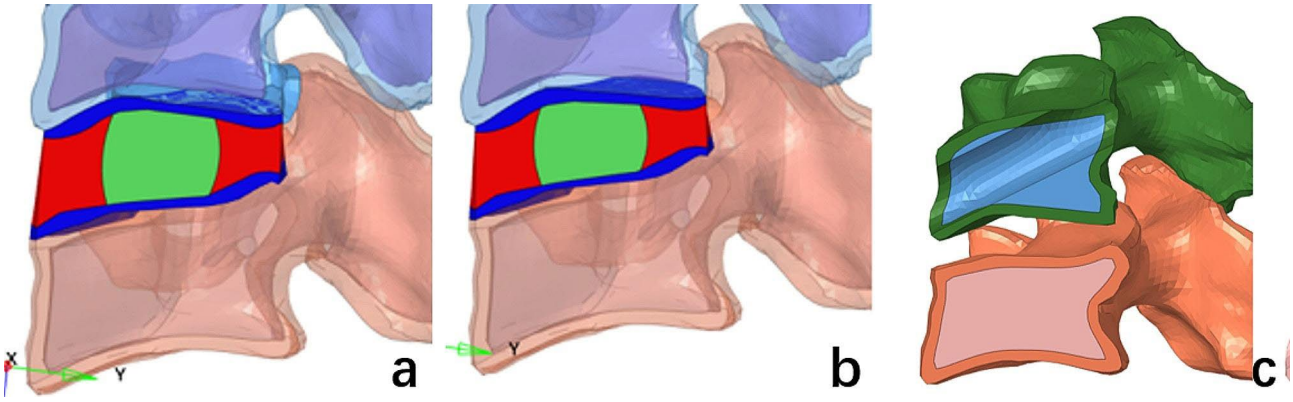

Fig. 2 Degenerative disc and bone channel FEM. (**a**) original disc height, (**b**) simulated post-disc degeneration height, (**c**) bone channel model

instability; (4) patients with coagulation dysfunction; (5) patients with a history of surgery on the same segment; (6) patients with severe spinal cord cervical spondylosis (Nurick grade IV or above). A total of 35 patients who underwent ATc-PECD between 2015 and 2016 were included in the study. All surgical procedures were performed by the same surgeon.

Surgery and follow up

The procedural details can be found in our previous study [11, 12]. Initially, the C-arm is utilized to determine the projection of the surgical vertebral body. The surgeon then employs the two-finger technique to create a safe gap between the carotid sheath and the visceral sheath. Under C-arm guidance, a Kirschner needle is fixed in the anterior lower part of the surgical vertebral body along this gap. A 7 mm incision is made in the surrounding skin at the Kirschner needle puncture point. A spreader is used to open the soft tissue channel along the path of the Kirschner needle, and then the working cannula is inserted along the spreader. After removing the spreader, a trephine (NOUVAG AG, Goldach, Switzerland) with an outer diameter of 7.5 mm is positioned to create a transcorporeal bone channel, closely monitored by the C-arm. When the trephine reaches the posterior superior edge of the targeted vertebral body, the central bone strip is gently removed by shaking the trephine. Upon establishment of the channel, a blunt hook was used to probe the posterior wall of the channel for penetration, followed by the use of pulpal forceps to remove the herniated disc. Finally, the posterior longitudinal ligament was broken open, and the return of dural sac expansion was observed as indicating the completion of decompression. All patients who underwent the surgery were followed up for at least 6 years.

Clinical evaluation

Changes in neck and arm pain were evaluated using the VAS. Neurological function was assessed using the JOA score. The improvement rate (IR) of the JOA score was used as a measure of surgical efficacy at the last follow-up visit, calculated as IR = (postoperative JOA score - preoperative JOA score) / (17 - preoperative JOA score) × 100%. Surgical outcomes were categorized as excellent (IR≥75%), good (75% > IR≥50%), fair (50% > IR≥25%), and poor (IR<25%) [11].

Radiologic evaluation

Imaging follow-up examinations consisted of MRI, computed tomography (CT), static and dynamic x-rays. MRI was used to assess recurrence of disc herniation and the effectiveness of surgical decompression, and CT was used to assess the healing of the vertebral bony channel. Cervical static lateral plain radiographs were utilized to evaluate intervertebral disc height (IDH) and vertebral body height (VBH). IDH refers to the linear distance from the center of the upper endplate to the center of the lower endplate of the intervertebral space, while VBH represents the linear distance from the center of the upper endplate to the center of the lower endplate of the vertebral body [41]. Cervical dynamic lateral radiographs were employed to assess cervical mobility and stability. Cervical ROM was the sum of the Cobb angle in extension and the Cobb angle in flexion. The Cobb angle is determined by two lines: the first line runs parallel to the bottom of the C2 vertebral body endplate, the second line runs parallel to the bottom of the C7 vertebral body endplate, and the angle of intersection between these two lines represents the Cobb angle [42].

Statistical analysis

The statistical analysis was conducted using the Statistical Package for Social Sciences (SPSS version 22.0, SPSS Inc., Chicago, IL). Paired samples t-tests were used to compare patients' VAS scores, JOA scores, IDH, VBH, and ROM during each follow-up period. Statistical significance was defined as a p-value≤0.05. The results are presented as mean±standard deviation (SD).

Results

Clinical results

A total of 35 patients who underwent ATc-PECD were included in the study. The demographics and clinical characteristics of the patients are presented in Table 2. Unlike previous short-term studies, this is the first study with a follow-up period of up to six years [13, 43, 44]. No postoperative complications reported. Following surgery, patients were required to wear a neck brace for a minimum of 3 weeks. Regular clinical evaluations were conducted during the 6-year follow-up period. At the final follow-up, most patients reported significant improvement in neurological symptoms compared to preoperative measurements. VAS and JOA scores are presented in Table 3, and the line graph is shown in Fig. 3. The last follow-up results showed a mean IR of 83.3% ± 14.6% (range: 60-100%). The clinical outcomes were classified as excellent in 28 cases (80%), good in 6 cases (17.1%), and fair in 1 case (2.9%).

FEM validation

The establishment of FEM involves two main steps: the construction of bone tissues and the construction of soft tissues. The reconstruction of bone tissues in FEM is similar to the process of CT three-dimensional reconstruction and requires original data such as CT scans or slices. The reconstruction of soft tissues is performed after the completion of bone tissue reconstruction, which these soft tissues are manually attached to the bone tissue

Table 2 Summary of patient demographics and clinical characteristics

Baseline characteristic	Value
Sex, male/female	19/16
Age (years)	50.14 ± 8.86 (35–69)
Duration of symptoms (weeks)	29.54 ± 15.11 (2–61)
Indication for surgery	
Myelopathy	18 (51.4%)
Radiculopathy	9 (25.7%)
Radiculopathy with myelopathy	8 (22.9%)
BMI	25.2 ± 2.8 (18.5–28.9)
Preoperative clinical features and signs	
Numbness in hands and decreased mobility	17 (48.6%)
Weakness of lower limbs	22 (62.9%)
Hoffman positive	9 (25.7%)
Knee hyperreflexia	11 (31.4%)
Bone Channel Establishment Segment	
C4 vertebrae	4 (13.3%)
C5 vertebrae	17 (56.7%)
C6 vertebrae	14 (46.6%)
Herniated disc size	
Sagittal height (mm)	9.30 ± 1.46 (7.43–13.95)
Sagittal width (mm)	5.65 ± 1.05 (3.77–7.33)
Coronal width (mm)	9.37 ± 1.95 (4.65–12.92)
Follow-up period (years)	7.10 ± 0.38 (6.30–7.80)
operative time (min)	**73.75 ± 11.28 (51–100)**
Post-operative length of stay (days)	**1.71 ± 0.85 (1–4)**

Values are number of patients (percentage) or mean ± SD (range)

model. Due to variations in the original data and the attachment methods of soft tissues such as ligaments, the ROM of models differs across different studies. There is no standard finite element model available for analysis. Validation of FEM involves comparing the established complete finite element model with the ROM of cervical spine from previous studies. As long as the differences in the ROM between model and those from previous models are not significant, the model construction approach is considered acceptable. To validate the FEM feasibility of our study, the completed model was imported into the commercial software Abaqus (version 6.10, Simulia, Providence, RI). The inferior surface of the T1 vertebra was constrained to prevent any displacement of the nodes. A non-destructive, purely rotational moment of 2 Nm was applied to the upper surface of the C2 vertebra in forward flexion, backward extension, lateral bending, and rotation. The predicted cervical range of motion (ROM) in each direction was recorded and compared to data from previously published studies [45–47]. The included studies consisted of one finite element study and two cadaveric experimental studies. The FEM of the included finite element studies were built with the same data sources and building methods that we used, while the cadaveric experiments were included with the purpose of observing the differences between the built FEMs and the real human body. The ROM predicted by the intact FEM does not deviate significantly from published findings (Fig. 4).

Imaging results

All patients underwent CT and MRI evaluations at 1 week and 6 years postoperatively to assess surgical outcomes and recurrence. The postoperative MRI at 1 week revealed complete decompression for all patients. At the 6-year postoperative MRI, only 1 patient demonstrated recurrence of CDH in the surgical segment, but the clinical symptoms were mild, and the patient's symptoms improved after conservative treatment. During the follow-up period, CT images showed no vertebral fractures or collapses in the operated segments, and all transcorporeal bone channels healed. Lateral dynamic radiograph of the cervical spine did not show cervical instability.

Case presentation

A 33-year-old man presented with right limb pain and numbness for 12+weeks. Strict conservative treatment was ineffective. On neurological examination, markedly numbness and decreased muscle strength (grade 3) was recorded on the right upper extremity. The Hoffman sign was positive in both upper extremities, with a visual analog scale (VAS) of 6 and a Japanese orthopedic association (JOA) score of 10. Magnetic resonance images (MRI) showed that para-central CDH at the C5/6 level. Postoperatively, the patient's symptoms improved significantly, MRI shows that the herniation did not recur, and CT shows that the patient's transcorporeal bone channel healed without vertebral body collapse or fracture. (Figures 5 and 6)

ROM changes of the cervical spine in the FEM and final radiologic examination

Dynamic radiographs were performed preoperatively, and at 1 year, 3 years, and 6 years postoperatively. And the results show that the patients' cervical ROM improved after surgery (Table 4), and the line graph is shown in Fig 7. On further analysis, we found that the increase in cervical spine ROM was mainly concentrated in the first year postoperatively ($P<0.05$), and there was no statistical difference in mobility between the groups at 1 year postoperatively, 3 years postoperatively, and 6 years postoperatively ($P>0.05$).

Comparing with the intact FEM, the cervical ROM in the degenerated disc FEM and the degenerated disc with surgical FEM was altered in each directions in the FEA (Table 5). The model demonstrated that cervical disc degeneration reduced the cervical ROM. However, after the establishment of bone channel, the ROM of the cervical spine increased in all directions. Specifically, in the C2-T1 FEM, the ROM increased from 45.592° to 46.635°

Table 3 Records of VAS and JOA score during the follow-up period

	Pre	1 month	1year	3year	6year
JOA	9.49 ± 2.16$^{\#\Delta}$	11.81 ± 1.80$^{*\Delta}$	14.37 ± 1.65$^{*\#}$	15.39 ± 1.54$^{*\#\Delta}$	15.71 ± 1.13$^{*\#\Delta}$
VAS					
Neck	6.34 ± 1.68$^{\#\Delta}$	3.51 ± 1.42$^{*\Delta}$	2.05 ± 0.96$^{*\#}$	1.34 ± 0.80$^{*\#\Delta}$	1.02 ± 0.82$^{*\#\Delta}$
Arm	5.14 ± 1.48$^{\#\Delta}$	2.57 ± 1.31$^{*\Delta}$	1.37 ± 0.91$^{*\#}$	0.83 ± 0.62$^{*\#\Delta}$	0.77 ± 0.76$^{*\#\Delta}$

Values are mean ± SD

* Compared with preoperative value, $P<0.05$; # compared with postoperative value at 1 month, $P<0.05$; Δ compared with postoperative value at 1year, $P<0.05$

Pre: preoperative; VAS: visual analog scale; JOA: Japanese Orthopedic Association

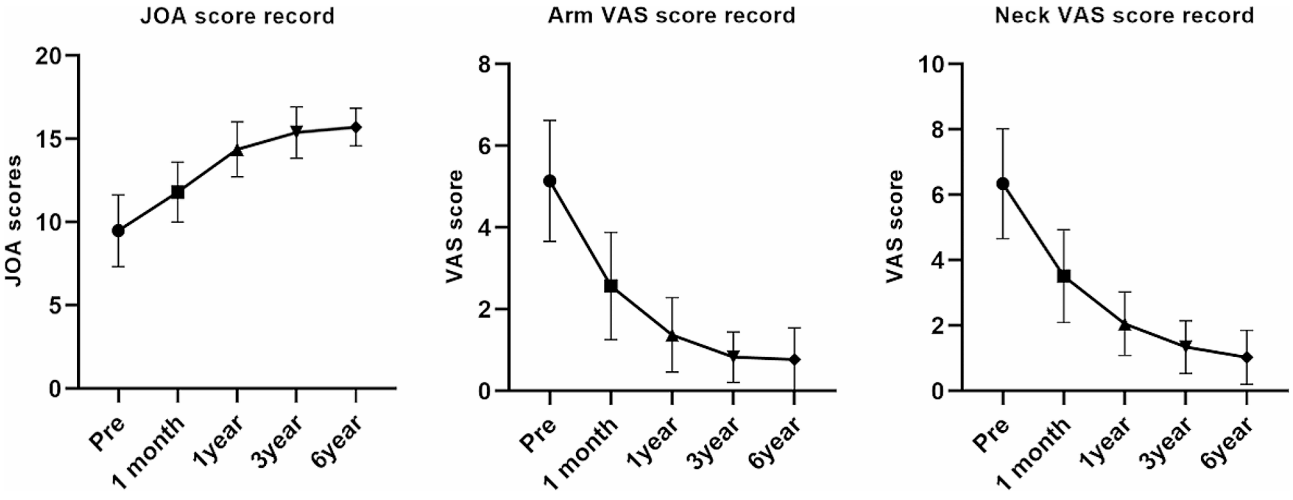

Fig. 3 The line graphs of changes in VAS and JOA score during follow-up

in flexion, from 27.018° to 27.668° in extension, from 33.373° to 33.651° in lateral bending, and from 40.271° to 40.759° in axial rotation. The augmentation of cervical flexion mobility at the C4-C5 segment constituted a remarkable 106% of the total increase in cervical flexion mobility. Likewise, the increments observed in extension, lateral bending, and rotational motion contributed to 105%, 87.4%, and 94.4% of the total increase, respectively. Conversely, the other segments displayed marginal or negligible changes in ROM across different directions.

Image changes after ATc-PECD and stress changes in FEM

The static radiographs showed that IDH and VBH progressively decreased after surgery in the operated segments. There was a statistically significant difference in IDH and VBH between preoperative, 1 year postoperative, 3 years postoperative and 6 years postoperative. ($P<0.05$) (Table 4), and the line graph is shown in Fig 7.

This study is the first to simultaneously analyses the stresses on the intervertebral disc and vertebral body after the establishment of a transcorporeal bony channel, and previous studies have often focused on only one of them, without comprehensively considering the changes in the stresses on both after the establishment of the bony channel [17, 20]. Disc degeneration and transcorporeal bone channel have a small effect on vertebral stress during cervical rotation, and lateral bending motions in the FEA. However, the establishment of transcorporeal bony channel increases intravertebral stresses during cervical extension (Fig. 8). We define the new stress concentrations due to structural changes in the cervical spine as abnormal stress concentrations. And the abnormal stress concentrations in the vertebral body primarily manifested at the entrance side wall of the channel during flexion and extension. There were no abnormal stress concentrations at the exit of the bone channel (Fig. 9).

Both cervical disc degeneration and transcorporeal bony channel can change intradiscal stress, and the transcorporeal bone channel was able to further increase the intradiscal stress in the degenerated disc model (Fig. 8). There were no abnormal stress concentrations found in the intervertebral disc during motion in all directions (Fig. 10).

As the changes in the applied stress can be involved in the remodeling of bone cells and disc degeneration. And there are FEA results showing that the vertebral body and intravertebral disc stresses will be further increased by surgery and degeneration modelling, so the reduction of IDH and VBH in patients may be related to the postoperative changes in internal cervical spine stresses [48, 49].

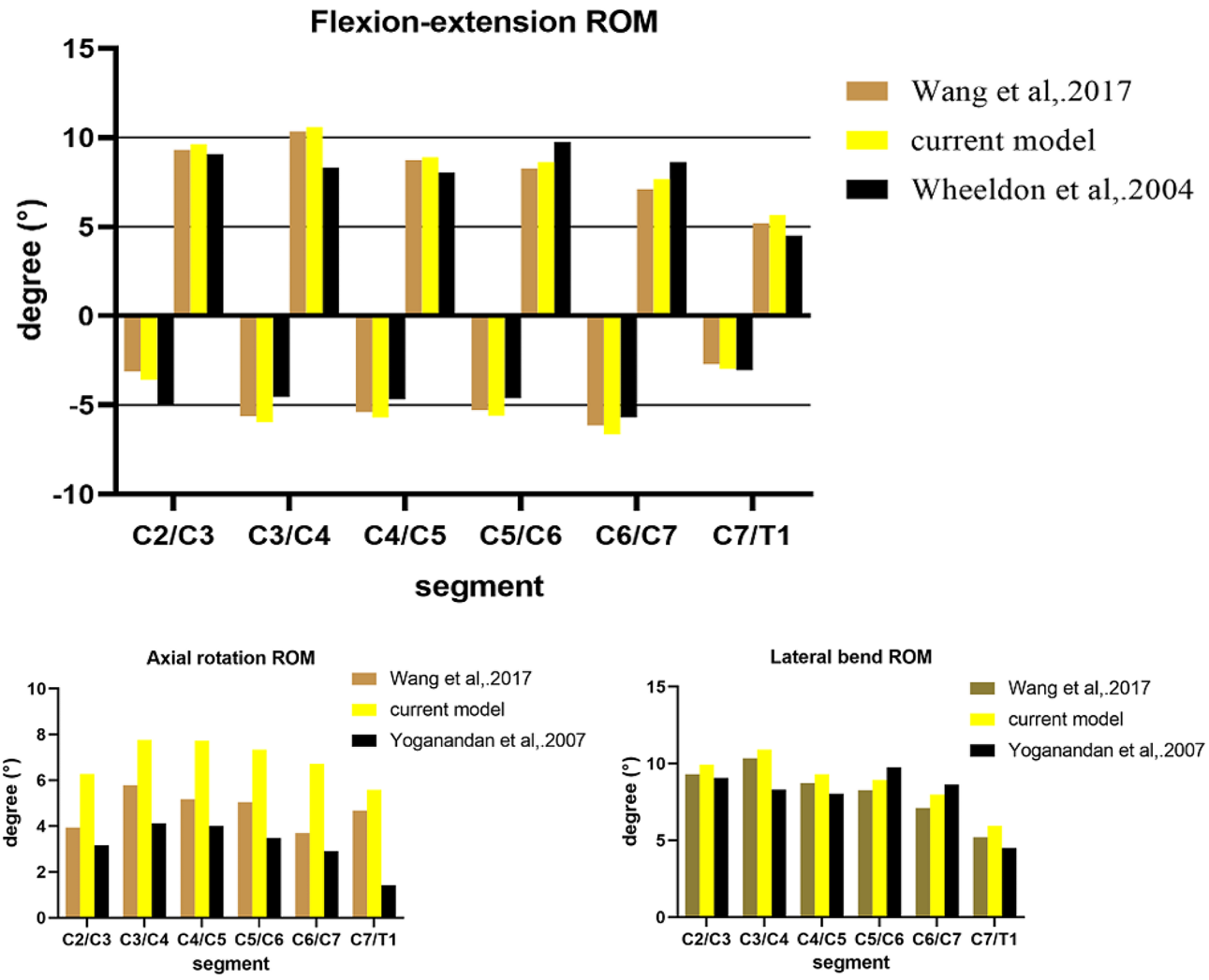

Fig. 4 This figure shows the predicted moment-rotation relationships of the FEM in the forward flexion (positive), back extension (negative), lateral bending, and axial rotation directions compared to the data in the literature

Discussion

The open surgery represented by ACDF is the main modality of CDH treatment at present, but open surgery may cause various complications such as vascular injury, nerve injury, adjacent segment degeneration, and cervical motion segment loss [50, 51]. As a result of a meta-analysis, the endoscopic-mediated minimally invasive surgery had a higher rate of excellent outcomes and lower operative and hospital stay compared to ACDF [52]. ATc-PECD represents a groundbreaking minimally invasive decompression technique for CDH [10]. Unlike the transdiscal approach, ATc-PECD is accomplished through bony channel in the vertebral body, which avoided damage to the anterior disc tissue. In a 2-year comparative study, although it was shown that both ATd-PECD and ATc-PECD can achieved patient-satisfying clinical outcomes, but the degree of IDH reduction and recurrence rate were significantly lower with the transcorporeal approach than with the transdiscal approach [18]. The bone channel caused a vertebral bone defect that changed the biomechanical conduction mechanism of the vertebral body, which inevitably leads to concerns among clinical orthopaedic surgeons that bone channeling will lead to vertebral collapse or fracture. Despite there have been a series of clinical reports of this technique, there are fewer studies of combined long-term clinical follow-up with cervical biomechanics after ATc-PECD. In this study, we analyzed the long-term biomechanical effects of transcorporeal bone channeling on the cervical spine by combining the results of long-term clinical follow-up and the results of FEA.

In our study, we employed transverse cryosections for FEM reconstruction. Previous research typically utilized CT or MRI for model reconstruction [53, 54]. However, these methods cannot adequately visualize both soft tissue and bone tissue simultaneously, and they sometimes

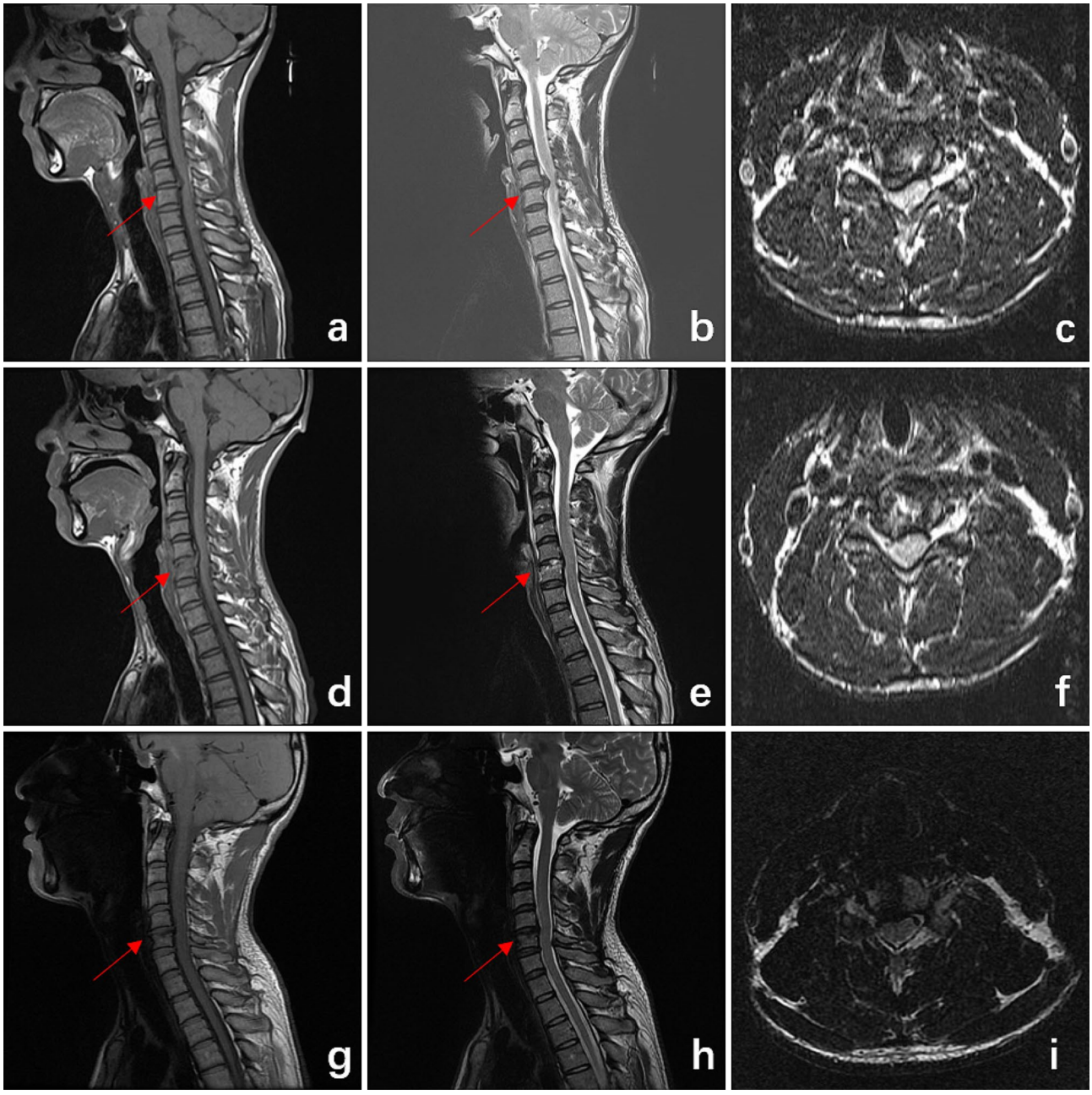

Fig. 5 Preoperative MRI showing disc herniation at C5/6 segments (**a**, **b**,**c**), the MRI images of the patient 1 week after surgery showed that the hernia mass was completely cleared (**d**, **e**, **f**), and the MRI images of the patient 6 years after surgery showed that the CDH no recurrent (**g**, **h**, **i**). T1 -weighted sagittal views (**a**, **d**, **g**). T2-weighted sagittal views (**b**, **e**, **h**). T1-weighted axial view (**c**, **f**, **i**)

fail to display certain anatomical details. Parts that cannot be visualized often require manual reconstruction, leading to artificial differences between the established models and real anatomical structures. Transverse cryosections provide genuine human anatomical cross-sectional images, presenting both bone and soft tissue clearly. Researchers can select the appropriate tissue for FEM reconstruction based on the focus of their study. In our research, when segmenting the original colour image we segment both the disc and the bone tissue. By importing the segmented original images into the computer, bone tissue and vertebral discs can be automatically reconstructed, thereby avoiding manual interference in the establishment of major structures.

The influencing factors of ROM after cervical spine surgery are diverse. The FEM results can only respond to the effects of structural changes to ROM, while the clinical follow-up can simultaneously respond to the effects of a variety of factors, including structural changes, pain relief, and the effect of postoperative recovery, which

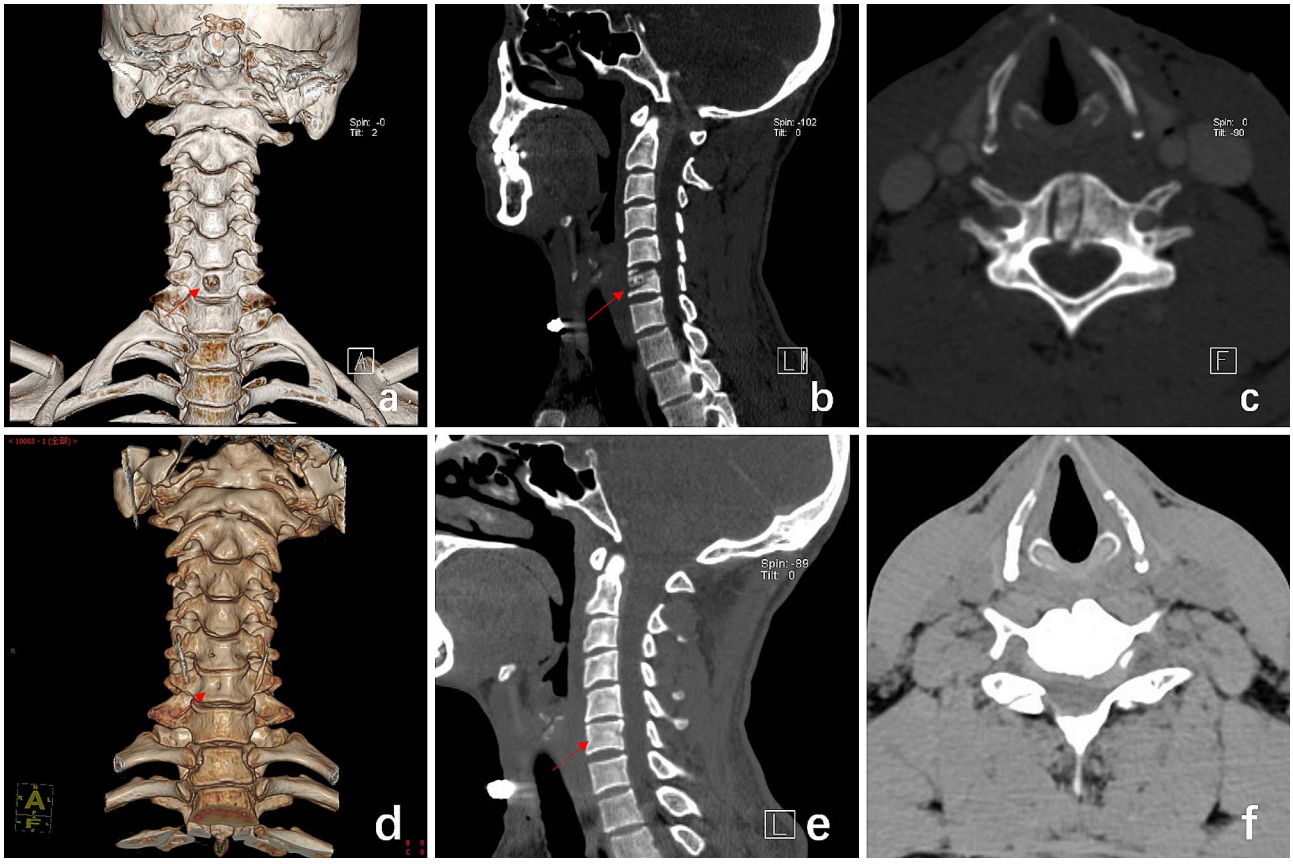

Fig. 6 CT images of the patient of follow-up visit. a, b, c are images at 1 week after surgery, and d, e, f are images at 6 years after surgery. (**a**) CT 3D reconstruction shows the location of the vertebral bone channel entrance. (**b**) Sagittal view shows the C6 vertebral bone channel and the internal autologous bone graft. (**c**) axial view shows the C6 vertebral bone channel and the internal autologous bone graft. (**d**) CT 3D reconstruction shows bony channel entrance healed at the patient's operated vertebral. (**e**) Sagittal view shows the C6 vertebral bone channel healed. (**f**) axial view shows the C6 vertebral bone channel healed

Table 4 Records of the changes of IDH, VBH, and ROM during the follow-up period

	Pre	1year	3year	6year
IDH (mm)	$5.95 \pm 0.22^{\#\Delta}$	$5.59 \pm 0.40^{*\Delta}$	$5.19 \pm 0.31^{*\#}$	$4.73 \pm 0.26^{*\#\Delta}$
VBH (mm)	$15.41 \pm 1.68^{\#\Delta}$	$15.05 \pm 1.65^{*\Delta}$	$14.35 \pm 1.64^{*\#}$	$13.67 \pm 1.48^{*\#\Delta}$
ROM (°)	$52.46 \pm 9.36^{\#\Delta}$	$58.91 \pm 6.68^{*}$	$58.71 \pm 6.84^{*}$	$59.26 \pm 6.72^{*}$

Values are mean ± SD

*Compared with preoperative value, $P<0.05$; #compared with postoperative value at 1year, $P<0.05$; Δcompared with postoperative value at 3year, $P<0.05$

Pre: preoperative; IDH: intervertebral disc height; VBH: vertebral body height; ROM: range of motion

collectively affect ROM. By analyzing the results of the follow-up, the patients exhibited a significant increase in cervical spine mobility only within the first year after surgery, with no statistically significant changes during the follow-up period beyond one year postoperatively. In addition, the two types of study also differed in the level of change in total cervical ROM after the establishment of transcorporeal bony channels, which in follow-up patients showed a more substantial change in ROM than FEA, suggests that the disruption of cervical structures can't fully explain increased cervical ROM. During the operation, we did not completely sever the anterior and posterior longitudinal ligaments. In the follow-up, we observed that the increased ROM of the cervical spine remained within the normal physiologic range, and no cervical instability occurred in the operated segments, which also proved that the surgical damage to the stable structures of the cervical spine was within the compensatory range. And the CT confirmed that all channel were able to obtain bone repair. Most importantly, the period of improvement in the patient's neck pain after surgery coincided with the period of increased cervical mobility after surgery. Based on the above analysis, the author posits that the pain relief and excellent recovery was another factor contributing to increased neck mobility,

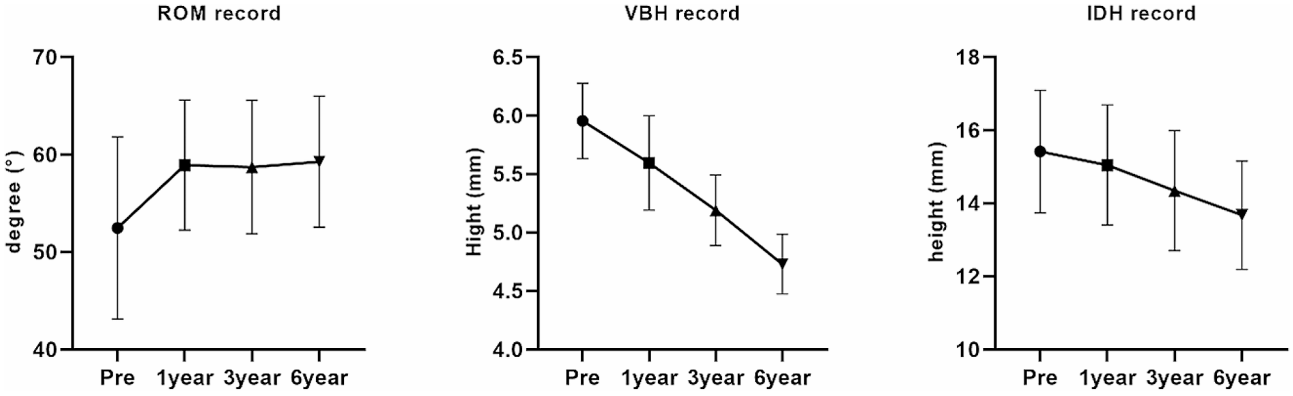

Fig. 7 The line graphs of changes in IDH, VBH, and ROM during follow-up

Table 5 Changes values in segmental and overall ROM of FEM pre- and post-disc degeneration, and pre- and post-establishment of bony channel

segment	flexion (°)		extension (°)		lateral bending (°)		axial rotation (°)	
	disc degeneration	bone channel	disc degeneration	bone channel	disc degeneration	bone channel	disc degeneration	bone channel
C2-T1	-3.298	0.843	-0.753	0.65	-3.852	0.278	-1.131	0.488
C2/3	-0.643 (19%)	-0.01 (-1%)	-0.4946 (66%)	0 (0%)	0.549 (-14%)	-0.019 (-7%)	1.681 (-149%)	0.011 (2%)
C3/4	-0.681 (21%)	-0.004 (1%)	0.9146 (-121%)	0.003 (1%)	-0.752 (20%)	-0.009 (-3%)	-0.166 (15%)	0.003 (1%)
C4/5	-0.441 (13%)	0.892 (106%)	0.161 (-21%)	0.677 (104%)	-1.148 (30%)	0.243 (87%)	-0.667 (59%)	0.371 (76%)
C5/6	-0.395 (12%)	-0.035 (-4%)	-0.457 (61%)	-0.03 (-5%)	-1.026 (27%)	0.063 (23%)	-0.457 (40%)	0.013 (3%)
C6/7	-0.469 (14%)	0 (0%)	-0.76 (101%)	0 (0%)	-0.612 (16%)	0 (0%)	-0.759 (67%)	0 (0%)
C7/T1	-0.669 (20%)	0 (0%)	-0.116 (15%)	0 (0%)	-0.863 (22%)	0 (0%)	-0.763 (67%)	0 (0%)

while the disruption caused by the surgical procedure is one of the causes.

In this study, we have provided further insights into the changes in vertebral body biomechanics following ATc-PECD, specifically highlighting the reduction of VBH in the operated segment. While Yu et al. [21]. were the first to observe decrease in VBH after ATc-PECD, but their follow-up period was limited to 2 years, which did not allow for further exploration of long-term changes in VBH. In the FEA study by WU et al [17], they focused mainly on analysing the effect of the diameter of the bone channel on the risk of fracture of the vertebral body in the postoperative, and did not combine it with postoperative clinical follow-up to study the long-term recovery of the patients. In our study, we extended the follow-up period and employed FEM to elucidate modifications in vertebral biomechanics subsequent to the establishment of the bone channel. We observed a sustained loss of VBH over a period of up to 6 years, and this result provides further strong evidence for changes in vertebral morphology after the establishment of transcorporeal bone channel. Additionally, our FEA of the vertebrae post ATc-PECD revealed stress concentration point coincides with the entrance to the bone channel, which may have implications for the remodeling and repair of the bone channel [48]. And lead to the reduction of VBH in the long-term postoperative period.

Disc degeneration is an irreversible process that can be accelerated by various factors, with disc injury being one of the primary causes, and numerous animal models have demonstrated that injury can induce intervertebral disc degeneration [55–57]. The surgical removal of a herniated disc unavoidably results in damage to the nucleus pulposus and posterior annulus fibrosus, consequently leading to disc degeneration. Additionally, changes in disc biomechanics contribute to the risk of disc degeneration. And the degenerated disc, in turn, further exacerbates biomechanical alterations, creating a vicious cycle [49]. IDH is a common consequence of disc degeneration, which is typically characterized by a reduction in intervertebral height [58]. In the FEM study by HE et al. [20]. they modelled the transcorporeal bone channel and observed the stress changes in the intervertebral disc. However, they did not model disc degeneration, so the simulation results did not take into account the effect of disc degeneration. The FEM employed in this study confirmed that cervical disc degeneration can increase internal stresses within the disc, and the establishment of bone channel can exacerbate this process. Consequently, the combination of these factors accelerates the disc degeneration. Early restoration of the biomechanical

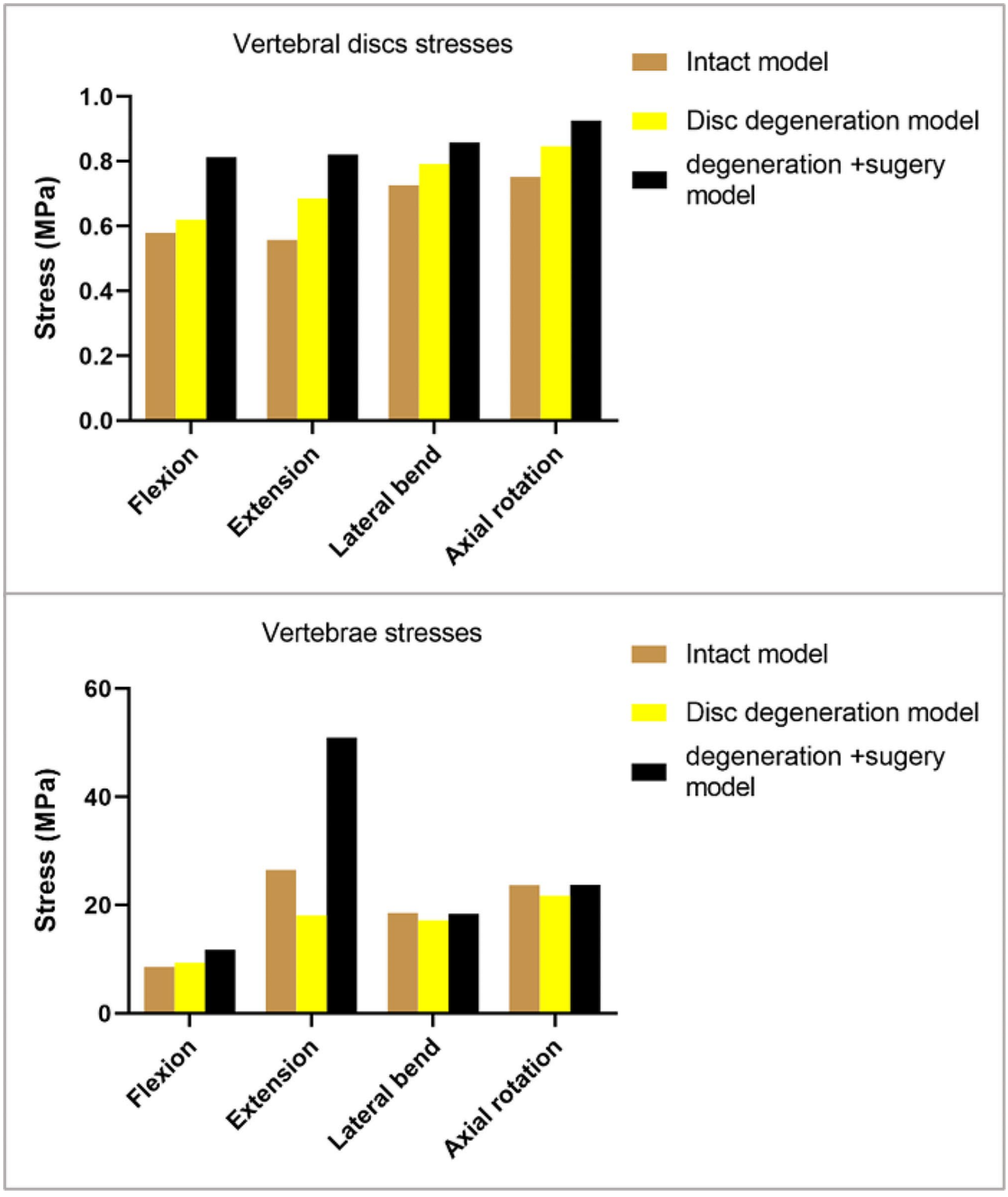

Fig. 8 Maximum stresses on the vertebral body and disc of the operated segment in each direction of motion for the intact FEM, the disc degeneration FEM, and the disc degeneration plus surgical FEM

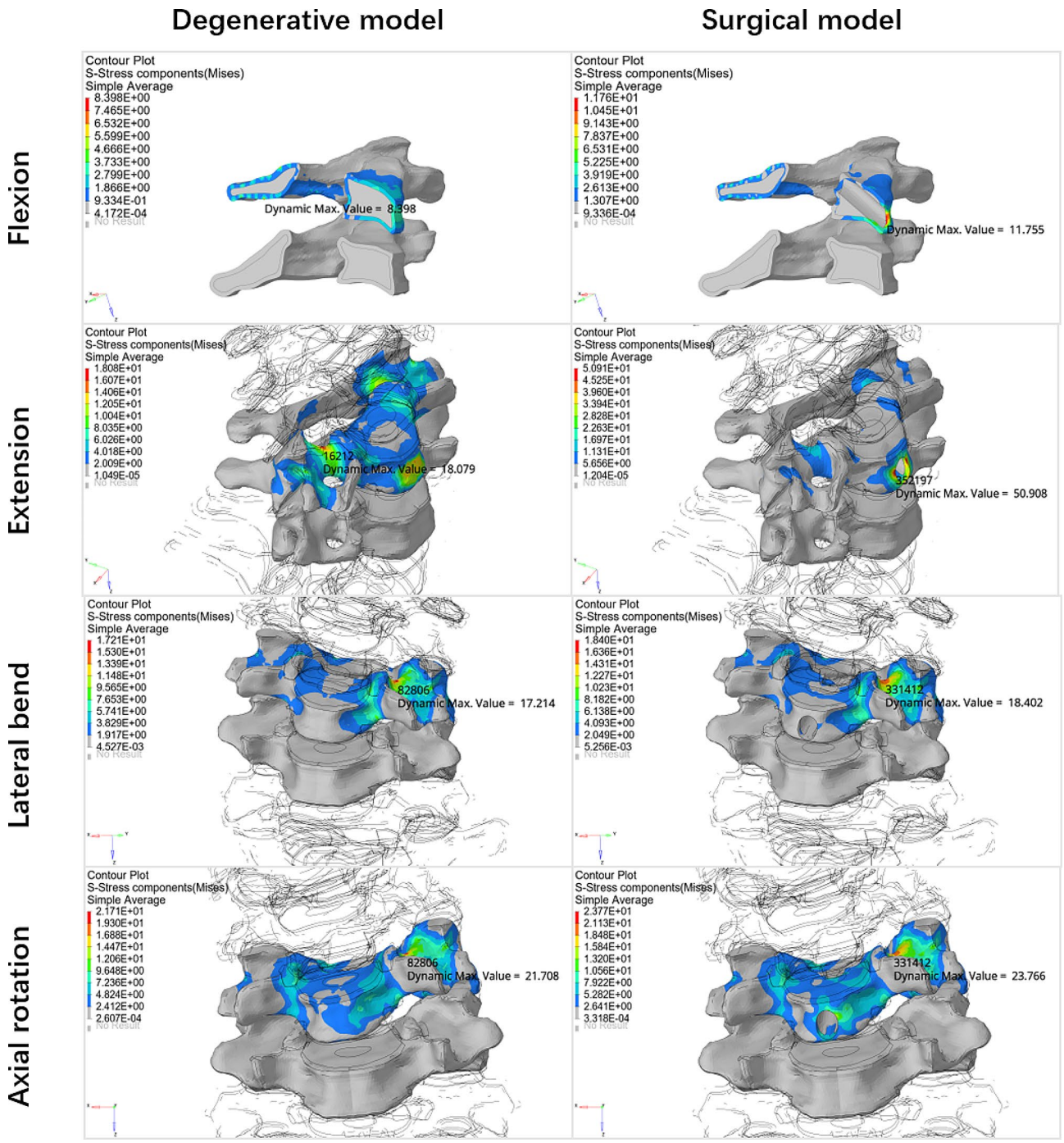

Fig. 9 Stress clouds of the vertebral body of the operated segment during flexion, extension, lateral bending, and axial rotation movements in the disc degeneration FEM and the disc degeneration plus surgery FEM

structure of the cervical spine may be the key to preventing a decrease in VBH and IDH. The surgeon may take the following measures. Firstly, promotion of bone channel restoration by bone grafting. Secondly, the size of the herniated disc should be adequately assessed preoperatively to create a bone channel of appropriate diameter and prevent the removal of excessive bone tissue. Finally, reduce the damage to stable structures such as ligaments.

There are also have some limitations to this study. The FEM original data for this study came from a Chinese woman, and the follow-up patients were all Chinese, so the applicability of the findings to other races needs to be further investigated. While our methodological approach

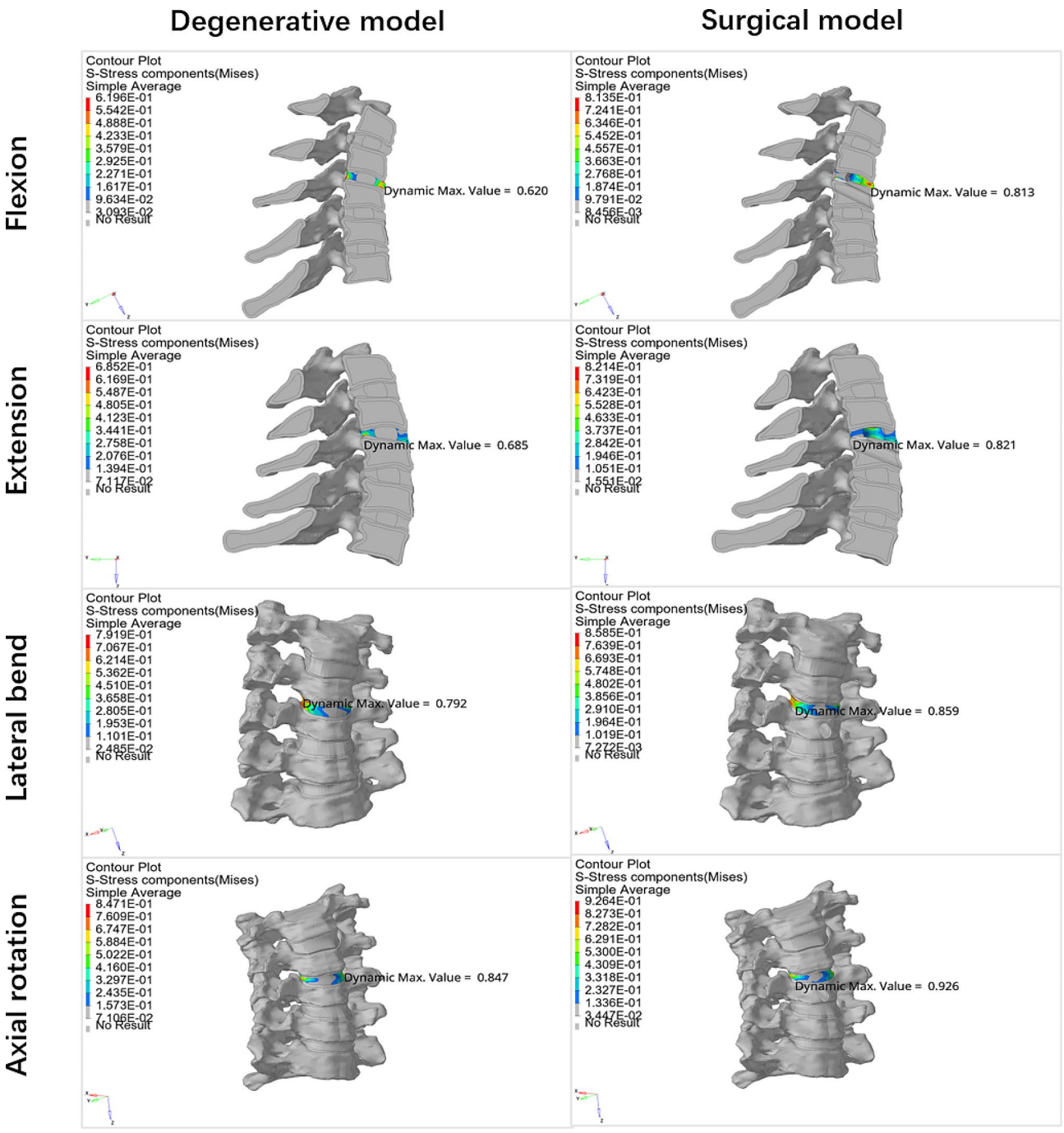

Fig. 10 Stress clouds of the operated segment discs during flexion, extension, lateral bending, and axial rotation movements in the disc degeneration FEM and the disc degeneration plus surgery FEM

of simulating disc degeneration through a reduction in disc height. Degeneration typically involves alterations in material properties of various spinal components, changes in bone quality, as well as modifications in the ligaments and soft tissues. We recognize that this simplification may not fully encapsulate the complex biomechanical and structural changes seen in a truly degenerative spine. Therefore, it's important to note that our model, while useful for initial investigations, may not completely represent the multifaceted nature of spinal degeneration. Measuring changes in the material properties of degenerated cervical spine tissues in future studies will hence better contribute to the accurate establishment of the FEM. In FEA, we used load control rather than displacement control, and while load control provides valuable insights, the model may not fully capture

the complex response of biological systems under natural movement conditions. Displacement control method is a new idea in cervical spine FEA research. Due to the variation in patient surgical segments and sample size limitations, we chose to assess the overall ROM of C2-C7 at the follow-up rather than analyzing individual surgical segment mobility. Therefore, we were unable to statistically analyse the changes in mobility of the cervical spine at the surgical segment, and the next step to expand the sample size and include patients with the same surgical segment is the key of our study.

Conclusion

Long-term follow-up studies have shown that ATc-PECD has good clinical efficacy and that ATc-PECD can be used as a complementary method for CDH treatment. The FEM demonstrated that ATc-PECD can lead to increased internal stresses in the vertebral body and intervertebral discs of the operated segments, which is directly related to cervical spine degeneration after ATc-PECD.

Abbreviations

ATc-PECD	Anterior percutaneous fully-endoscopic transcorporeal decompression
CDH	Cervical disc herniation
CT	Computed tomography
FEA	Finite element analysis
FEM	Finite element model
IDH	Intervertebral disc height
IR	Improvement rate
JOA	Japanese orthopaedic association
MRI	Magnetic resonance imaging
PECD	Percutaneous endoscopic cervical discectomy
ROM	Range of motion
VAS	Visual analog scale
VBH	Vertebral body height

Acknowledgements

I would like to thank my mentor Wenbo Liao for his carefully modifying the manuscript. Thanks to my family for their support.

Author contributions

KWJ and LWB designed and directed the study, and DQ and WZJ were the executors of the finite element modeling, collection of follow-up data, and writing of the manuscript. ZHD and WSF were involved in the collection of follow-up data and the analysis of the data. CGR, XZJ, and ZMB assisted in the patient's surgeries as assistants, as well as delineating the original color images for the creation of the FEM. All surgeries were performed by KWJ and LWB.

Funding

Guizhou Provincial Health Commission, Science and Technology Fund (gzwkj2022-196).
Basic Research Program of Department of Science and Technology (Qiankehe Foundation-ZK [2024] General-347)
Collaborative Innovation Center of Chinese Ministry of Education (Grant number:2020-39).

Data availability

The datasets generated and/or analysed during the current study are not publicly available due [REASON WHY DATA ARE NOT PUBLIC] but are available from the corresponding author on reasonable request.

Declarations

Ethics approval and consent to participate

This study approved by the Ethics Committee of The Affiliated Hospital of Zunyi Medical University (KLL-2021-319) in December 2021. All patients signed informed consent forms. All methods were performed in accordance with the relevant guidelines and regulations.

Consent for publication

Not Applicable.

Competing interests

The authors declare no competing interests.

Author details

[1]Department of Orthopedics, The Second Affiliated Hospital of Zunyi Medical University, ZunYi 563000, China
[2]Department of Spinal Surgery, The Affiliated Hospital of Zunyi Medical University, ZunYi 563000, China
[3]The Collaborative Innovation Center of Tissue Damage Repair and Regeneration Medicine of Zunyi Medical University, ZunYi 563000, China

Received: 14 November 2023 / Accepted: 1 August 2024
Published online: 13 August 2024

References

1. Wu B, Yang L, Fu C, Zhuo Y, Feng X, Xiong H. Global trends and hotspots in endoscopic discectomy: a study based on bibliometric analysis. Neurospine. 2022;19:1093–107. https://doi.org/10.14245/ns.2244574.287
2. Ahn Y, Lee SH, Chung SE, Park HS, Shin SW. Percutaneous endoscopic cervical discectomy for discogenic cervical headache due to soft disc herniation. Neuroradiology. 2005;47:924–30. https://doi.org/10.1007/s00234-005-1436-y
3. Ruetten S, Komp M, Merk H, Godolias G. Full-endoscopic anterior decompression versus conventional anterior decompression and fusion in cervical disc herniations. Int Orthop. 2009;33:1677–82. https://doi.org/10.1007/s00264-008-0684-y
4. Yang JS, Chu L, Chen L, Chen F, Ke ZY, Deng ZL. Anterior or posterior approach of full-endoscopic cervical discectomy for cervical intervertebral disc herniation? A comparative cohort study. Spine (Phila Pa 1976). 2014;39:1743–50. https://doi.org/10.1097/brs.0000000000000508
5. Ruetten S, Komp M, Merk H, Godolias G. A new full-endoscopic technique for cervical posterior foraminotomy in the treatment of lateral disc herniations using 6.9-mm endoscopes: prospective 2-year results of 87 patients. Minim Invasive Neurosurg. 2007;50:219–26. https://doi.org/10.1055/s-2007-985860
6. George B, Zerah M, Lot G, Hurth M. Oblique transcorporeal approach to anteriorly located lesions in the cervical spinal canal. Acta Neurochir (Wien). 1993;121:187–90. https://doi.org/10.1007/bf01809273
7. Jho HD. Microsurgical anterior cervical foraminotomy for radiculopathy: a new approach to cervical disc herniation. J Neurosurg. 1996;84:155–60. https://doi.org/10.3171/jns.1996.84.2.0155
8. Jho HD, Kim WK, Kim MH. Anterior microforaminotomy for treatment of cervical radiculopathy: part 1–disc-preserving functional cervical disc surgery. Neurosurgery. 2002;51:S46–53.
9. Umebayashi D, Hara M, Nakajima Y, Nishimura Y, Wakabayashi T. Transvertebral anterior cervical foraminotomy: midterm outcomes of clinical and radiological assessments including the finite element method. Eur Spine J. 2013;22:2884–90. https://doi.org/10.1007/s00586-013-2974-3
10. Deng ZL, Chu L, Chen L, Yang JS. Anterior transcorporeal approach of percutaneous endoscopic cervical discectomy for disc herniation at the C4-C5 levels: a technical note. Spine J. 2016;16:659–66. https://doi.org/10.1016/j.spinee.2016.01.187
11. Du Q, Wang X, Qin JP, Friis T, Kong WJ, Cai YQ, Ao J, Xu H, Liao WB. Percutaneous full-endoscopic anterior transcorporeal procedure for cervical disc herniation: a novel procedure and early follow-up study. World Neurosurg. 2018;112:e23–30. https://doi.org/10.1016/j.wneu.2017.12.001
12. Ma Y, Xin Z, Kong W, Zhang L, Du Q, Liao W. Transcorporeal decompression using a fully-endoscopic anterior cervical approach to treat cervical spondylotic myelopathy: surgical design and clinical application. BMC Musculoskelet Disord. 2022;23:1031. https://doi.org/10.1186/s12891-022-06001-5

13. Chen X, Gao JA, Du Q, Qiao Y, Kong WJ, Liao WB. Percutaneous full-endoscopic anterior transcorporeal cervical discectomy for the treatment of cervical disc herniation: surgical design and results. Pain Physician. 2021;24:E811–9.
14. Kong W, Xin Z, Du Q, Cao G, Liao W. Anterior percutaneous full-endoscopic transcorporeal decompression of the spinal cord for single-segment cervical spondylotic myelopathy: the technical interpretation and 2 years of clinical follow-up. J Orthop Surg Res. 2019;14:461. https://doi.org/10.1186/s13018-019-1474-5
15. Walter BA, Korecki CL, Purmessur D, Roughley PJ, Michalek AJ, Iatridis JC. Complex loading affects intervertebral disc mechanics and biology. Osteoarthritis Cartilage. 2011;19:1011–8. https://doi.org/10.1016/j.joca.2011.04.005
16. Imamura K, Ozawa H, Hiraide T, Takahashi N, Shibasaki Y, Fukuhara T, Suda T. Continuously applied compressive pressure induces bone resorption by a mechanism involving prostaglandin E2 synthesis. J Cell Physiol. 1990;144:222–8. https://doi.org/10.1002/jcp.1041440207
17. Wu WK, Yan ZJ, Zhang TF, Liao CG, Liang KL, Chen L, Deng ZL. Biomechanical influences of transcorporeal tunnels on c4 vertebra under physical compressive load under flexion movement: a finite element analysis. World Neurosurg. 2018;114:e199–208. https://doi.org/10.1016/j.wneu.2018.02.140
18. Ren Y, Yang J, Chen CM, Liu K, Wang XF, Wei JM, Shi L, Liu W, Jiang H, Zhou H et al. Outcomes of discectomy by using full-endoscopic visualization technique via the transcorporeal and transdiscal approaches in the treatment of cervical intervertebral disc herniation: a comparative study. BioMed research international. 2020;2020:5613459. https://doi.org/10.1155/2020/5613459
19. Ke W, Zhi J, Hua W, Wang B, Lu S, Fan L, Li L, Yang C. Percutaneous posterior full-endoscopic cervical foraminotomy and discectomy: a finite element analysis and radiological assessment. Comput Methods Biomech Biomed Engin. 2020;23:805–14. https://doi.org/10.1080/10255842.2020.1765162
20. He T, Zhang J, Yu T, Wu J, Yuan T, Liu R, Yun Z, Du H, Qi L, An J, et al. Comparative analysis of the biomechanical characteristics after different minimally invasive surgeries for cervical spondylopathy: a finite element analysis. Front Bioeng Biotechnol. 2021;9:772853. https://doi.org/10.3389/fbioe.2021.772853
21. Yu KX, Chu L, Yang JS, Deng R, Chen L, Shi L, Hao DJ, Deng ZL. Anterior transcorporeal approach to percutaneous endoscopic cervical diskectomy for single-level cervical intervertebral disk herniation: case series with 2-year follow-up. World Neurosurg. 2019;122:e1345–53. https://doi.org/10.1016/j.wneu.2018.11.045
22. Wang Z, Zhao H, Liu JM, Tan LW, Liu P, Zhao JH. Resection or degeneration of uncovertebral joints altered the segmental kinematics and load-sharing pattern of subaxial cervical spine: a biomechanical investigation using a C2-T1 finite element model. J Biomech. 2016;49:2854–62. https://doi.org/10.1016/j.jbiomech.2016.06.027
23. Panjabi MM, Shin EK, Chen NC, Wang JL. Internal morphology of human cervical pedicles. Spine (Phila Pa 1976). 2000;25:1197–205. https://doi.org/10.1097/00007632-200005150-00002
24. Panjabi MM, Chen NC, Shin EK, Wang JL. The cortical shell architecture of human cervical vertebral bodies. Spine (Phila Pa 1976). 2001;26:2478–84. https://doi.org/10.1097/00007632-200111150-00016
25. Womack W, Woldtvedt D, Puttlitz CM. Lower cervical spine facet cartilage thickness mapping. Osteoarthritis Cartilage. 2008;16:1018–23. https://doi.org/10.1016/j.joca.2008.01.007
26. Wong CE, Hu HT, Hsieh MP, Huang KY. Optimization of three-level cervical hybrid surgery to prevent adjacent segment disease: a finite element study. Front Bioeng Biotechnol. 2020;8:154. https://doi.org/10.3389/fbioe.2020.00154
27. Leahy PD, Puttlitz CM. The effects of ligamentous injury in the human lower cervical spine. J Biomech. 2012;45:2668–72. https://doi.org/10.1016/j.jbiomech.2012.08.012
28. Wu TK, Meng Y, Liu H, Wang BY, Hong Y, Rong X, Ding C, Chen H. Biomechanical effects on the intermediate segment of noncontiguous hybrid surgery with cervical disc arthroplasty and anterior cervical discectomy and fusion: a finite element analysis. Spine J. 2019;19:1254–63. https://doi.org/10.1016/j.spinee.2019.02.004
29. Hua W, Zhi J, Ke W, Wang B, Yang S, Li L, Yang C. Adjacent segment biomechanical changes after one- or two-level anterior cervical discectomy and fusion using either a zero-profile device or cage plus plate: a finite element analysis. Comput Biol Med. 2020;120:103760. https://doi.org/10.1016/j.compbiomed.2020.103760
30. Wheeldon JA, Stemper BD, Yoganandan N, Pintar FA. Validation of a finite element model of the young normal lower cervical spine. Ann Biomed Eng. 2008;36:1458–69. https://doi.org/10.1007/s10439-008-9534-8
31. Schmidt H, Heuer F, Simon U, Kettler A, Rohlmann A, Claes L, Wilke HJ. Application of a new calibration method for a three-dimensional finite element model of a human lumbar annulus fibrosus. Clin Biomech. 2006;21:337–44. https://doi.org/10.1016/j.clinbiomech.2005.12.001
32. Kallemeyn N, Gandhi A, Kode S, Shivanna K, Smucker J, Grosland N. Validation of a C2-C7 cervical spine finite element model using specimen-specific flexibility data. Med Eng Phys. 2010;32:482–9. https://doi.org/10.1016/j.medengphy.2010.03.001
33. Shirazi-Adl A, Ahmed AM, Shrivastava SC. Mechanical response of a lumbar motion segment in axial torque alone and combined with compression. Spine (Phila Pa 1976). 1986;11:914–27. https://doi.org/10.1097/00007632-198611000-00012
34. Holzapfel GA, Schulze-Bauer CA, Feigl G, Regitnig P. Single lamellar mechanics of the human lumbar anulus fibrosus. Biomech Model Mechanobiol. 2005;3:125–40. https://doi.org/10.1007/s10237-004-0053-8
35. Yoganandan N, Kumaresan S, Pintar FA. Geometric and mechanical properties of human cervical spine ligaments. J Biomech Eng. 2000;122:623–9. https://doi.org/10.1115/1.1322034
36. Yoganandan N, Kumaresan S, Pintar FA. Biomechanics of the cervical spine part 2. Cervical spine soft tissue responses and biomechanical modeling. Clin Biomech. 2001;16:1–27. https://doi.org/10.1016/s0268-0033(00)00074-7
37. Liu Y, Zhao Z, Guo C, Huang Z, Zhang W, Ma F, Wang Z, Kong Q, Wang Y. Application and development of hydrogel biomaterials for the treatment of intervertebral disc degeneration: a literature review. Front cell Dev Biology. 2023;11:1286223. https://doi.org/10.3389/fcell.2023.1286223
38. Wang Z, Li X, Yu P, Zhu Y, Dai F, Ma Z, Shen X, Jiang H, Liu J. Role of autophagy and pyroptosis in intervertebral disc degeneration. J Inflamm Res. 2024;17:91–100. https://doi.org/10.2147/jir.S434896
39. Du Q, Zhang MB, Kong WJ, Cao GR, Xin ZJ, Fu ZH, Liao WB. A novel technique of endoscopic anterior transcorporeal approach with channel repair for adjacent segment disease after anterior cervical discectomy and fusion. World Neurosurg. 2021;154:109–16. https://doi.org/10.1016/j.wneu.2021.07.038
40. Du Q, Lei LQ, Cao GR, Kong WJ, Ao J, Wang X, Wang AS, Liao WB. Percutaneous full-endoscopic anterior transcorporeal cervical discectomy and channel repair: a technique note report. BMC Musculoskelet Disord. 2019;20:280. https://doi.org/10.1186/s12891-019-2659-0
41. Asai T, Sakuma E, Mizutani T, Ishizaka Y, Ori K, Ueki T. Sex- and age-related differences in spinal degeneration: an anatomical and magnetic resonance imaging study of the human spine. Progress Rehabilitation Med. 2022;7:20220011. https://doi.org/10.2490/prm.20220011
42. Kozaki T, Yukawa Y, Hashizume H, Iwasaki H, Tsutsui S, Takami M, Nagata K, Taiji R, Murata S, Yamada H. Clinical and radiographic characteristics of increased signal intensity of the spinal cord at the vertebral body level in patients with cervical myelopathy. J Orthop Sci. 2023;28:1240–5. https://doi.org/10.1016/j.jos.2022.10.010
43. Yang J, Chu L, Deng Z, Kai-Xuan L, Deng R, Chen H, Liu P, Liu T, Rong X, Hao D. Clinical study of single-level cervical disc herniation treated by full-endoscopic decompression via anterior transcorporeal approach. Zhongguo Xiu Fu Chong Jian Wai Ke Za Zhi. 2020;34:543–9. https://doi.org/10.7507/1002-1892.201905118
44. Yanyan M, Zhijun X, Weijun K, Longsheng Z, Qian D, Wenbo L. Correction: transcorporeal decompression using a fully-endoscopic anterior cervical approach to treat cervical spondylotic myelopathy: surgical design and clinical application. BMC Musculoskelet Disord. 2023;24:68. https://doi.org/10.1186/s12891-023-06180-9
45. Wang Z, Zhao H, Liu JM, Chao R, Chen TB, Tan LW, Zhu F, Zhao JH, Liu P. Biomechanics of anterior plating failure in treating distractive flexion injury in the caudal subaxial cervical spine. Clin Biomech. 2017;50:130–8. https://doi.org/10.1016/j.clinbiomech.2017.10.017
46. Wheeldon JA, Pintar FA, Knowles S, Yoganandan N. Experimental flexion/extension data corridors for validation of finite element models of the young, normal cervical spine. J Biomech. 2006;39:375–80. https://doi.org/10.1016/j.jbiomech.2004.11.014
47. Yoganandan N, Pintar FA, Stemper BD, Wolfla CE, Shender BS, Paskoff G. Level-dependent coronal and axial moment-rotation corridors of degeneration-free cervical spines in lateral flexion. J Bone Joint Surg Am. 2007;89:1066–74. https://doi.org/10.2106/jbjs.F.00200
48. Liu P, Tu J, Wang W, Li Z, Li Y, Yu X, Zhang Z. Effects of mechanical stress stimulation on function and expression mechanism of osteoblasts. Front Bioeng Biotechnol. 2022;10:830722. https://doi.org/10.3389/fbioe.2022.830722
49. Vergroesen PP, Kingma I, Emanuel KS, Hoogendoorn RJ, Welting TJ, van Royen BJ, van Dieën JH, Smit TH. Mechanics and biology in intervertebral

disc degeneration: a vicious circle. Osteoarthritis Cartilage. 2015;23:1057–70. https://doi.org/10.1016/j.joca.2015.03.028
50. Matsumoto M, Okada E, Ichihara D, Watanabe K, Chiba K, Toyama Y, Fujiwara H, Momoshima S, Nishiwaki Y, Iwanami A, et al. Anterior cervical decompression and fusion accelerates adjacent segment degeneration: comparison with asymptomatic volunteers in a ten-year magnetic resonance imaging follow-up study. Spine (Phila Pa 1976). 2010;35:36–43. https://doi.org/10.1097/BRS.0b013e3181b8a80d
51. Sugawara T. Anterior cervical spine surgery for degenerative disease: a review. Neurol Med Chir (Tokyo). 2015;55:540–6. https://doi.org/10.2176/nmc.ra.2014-0403
52. Zhang J, Zhou Q, Yan Y, Ren J, Wei S, Zhu H, Song Z. Efficacy and safety of percutaneous endoscopic cervical discectomy for cervical disc herniation: a systematic review and meta-analysis. J Orthop Surg Res. 2022;17:519. https://doi.org/10.1186/s13018-022-03365-1
53. Yoganandan N, Harinathan B, Vedantam A. Cervical column and cord and column responses in whiplash with stenosis: a finite element modeling study. J Eng Sci Med Diagnostics Therapy. 2024;7:021003. https://doi.org/10.1115/1.4063250
54. Kong Q, Li F, Yan C, Sun J, Sun P, Ou-Yang J, Zhong S, Wang Y, Shi J. Biomechanical comparison of anterior cervical corpectomy decompression and fusion, anterior cervical discectomy and fusion, and anterior controllable antedisplacement and fusion in the surgical treatment of multilevel cervical spondylotic myelopathy: a finite element analysis. Orthop Surg. 2024;16:687–99. https://doi.org/10.1111/os.13994
55. Kim KS, Yoon ST, Li J, Park JS, Hutton WC. Disc degeneration in the rabbit: a biochemical and radiological comparison between four disc injury models. Spine (Phila Pa 1976). 2005;30:33–7. https://doi.org/10.1097/01.brs.0000149191.02304.9b
56. Rousseau MA, Ulrich JA, Bass EC, Rodriguez AG, Liu JJ, Lotz JC. Stab incision for inducing intervertebral disc degeneration in the rat. Spine (Phila Pa 1976). 2007;32:17–24. https://doi.org/10.1097/01.brs.0000251013.07656.45
57. Zhang Y, Drapeau S, An HS, Markova D, Lenart BA, Anderson DG. Histological features of the degenerating intervertebral disc in a goat disc-injury model. Spine (Phila Pa 1976). 2011;36:1519–27. https://doi.org/10.1097/BRS.0b013e3181f60b39
58. Li Y, Chen L, Gao Y, Zou X, Wei F. Oxidative stress and intervertebral disc degeneration: pathophysiology, signaling pathway, and therapy. Oxid Med Cell Longev. 2022;2022:1984742. https://doi.org/10.1155/2022/1984742

Publisher's Note

Springer Nature remains neutral with regard to jurisdictional claims in published maps and institutional affiliations.